Performance Characteristics of Semi-Active and Passive Damper using Different Car Models

Sivakoteswararao Ikkurthi

A Thesis Submitted to

Indian Institute of Technology Hyderabad

In Partial Fulfillment of the Requirements for

The Degree of Master of Technology

Department of Mechanical and Aerospace Engineering

July 2015

Declaration

I declare that this written submission represents my ideas in my own words, and where ideas or words of others have been included, I have adequately cited and referenced the original sources. I also declare that I have adhered to all principles of academic honesty and integrity and have not misrepresented or fabricated or falsified any idea/data/fact/source in my submission. I understand that any violation of the above will be a cause for disciplinary action by the Institute and can also evoke penal action from the sources that have thus not been properly cited, or from whom proper permission has not been taken when needed.

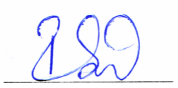

(Signature)

SIVAKOTESWARARAO IKKURTHI

(Sivakoteswararao Ikkurthi)

ME13M1014

(Roll No.)

Approval Sheet

This Thesis entitled Performance Characteristics of Semi-Active and Passive Damper using Different Car Models by Sivakoteswararao Ikkurthi is approved for the degree of Master of Technology from IIT Hyderabad

(Ketan P Detroja) Examiner
Dept. of Electrical Eng.
IITM

(R Prasanth Kumar) Examiner
Dept. of Mechanical and Aerospace Eng.
IITH

(Ashok Kumar Pandey) Adviser
Dept. of Mechanical and Aerospace Eng.
IITH

(Ketan P Detroja) Chairman
Dept. of Electrical Eng.
IITH

Acknowledgements

I would like to thank all the people who have guided and supported me throughout my thesis work. First of all, I express my immense gratitude to my advisor Dr. Ashok Kumar Pandey, for giving me valuable guidance and directions all the time during my thesis work. I also thank him for mentoring me in such an interesting field of vehicle dynamics and believing in me during the research work. I also thank him for his excellent advises, guidance and all time valuable support and encouragement.

I would like to extend my gratitude to my committee members who have made interesting and useful remarks during my thesis work. I also wish to thank Professor V. Eswaran, H.O.D, Department of Mechanical Engineering, IIT Hyderabad for his support during my Mtech program and Professor U.B Desai, Director, IIT Hyderabad for their support in various ways. I acknowledge all the faculty members of Mechanical Engg. Dept., IIT Hyderabad, specially Dr. R. Prasanth Kumar, Dr. C. P. Vyasarayani, Dr. M. Ramji, Dr. B. Venkatesham, Dr. V. Chinthapenta for giving me valuable technical details in the subjects i studied during my course work. These techniques helped me directly or indirectly in completing my thesis work. Also i would like to express my gratitude to Dr. Ketan, from electrical department for giving valuable knowledge on control engineering area which is helpful in the thesis work. I must not ignore the special contributions of the institute library for providing all the necessary books, articles and access to many useful domains to enrich my asset list in this research work.

Many, many thanks go to my family for their blessings and support. I wish to thank my father and mother for supporting me during my studies in various ways. I wish to express my special thanks to my wife Mrs. Indira Mokhamatam for her support for continuing my studies and taking care of the family. I am also thankful to my IIT Hyderabad friends for the warmth of their friendship and providing a supportive environment, which has made my stay at IIT Hyderabad wonderful. I sincerely acknowledge my group mates Bimal, Bibin and Aparna for their role in supporting me in different ways. I would also like to acknowledge Mr. Prashant Kambli and Anwar sadat, Ph.D.. Scholars, IIT Hyderabad, for their support and help in giving suggestions for solving papers during the thesis work.

Dedication

To my wife Indira

Abstract

Comfort performance of any vehicle depends on the dynamic characteristics of dampers. In this thesis, we analyze the influence of semi-active MR(Magnetorheological) damper using the quarter and half car models, and discuss about the nonlinear characteristics of passive oil damper using half car model. The vehicle suspension of quarter car model with MR damper is considered while the vehicle is travelling at constant speed on random road profile. The hysteretic behaviour of the MR damper is characterized using modified Bouc-Wen model. Using equivalent linearization technique hysteretic behaviour of MR damper is linearized and used in the state space form. Subsequently, the rms values of system response characteristics such as sprung mass acceleration, suspension stroke, road holding and control force verses vehicle velocity are obtained by solving matrix lyapunov equation in time domain. The system response in term of above parameters are computed for the parameters related with MR damper at different current which are obtained from the experimental conducted in our group. It is found that as the current in MR damper increases, the control force also increases, thus, reducing the suspension stroke and road holding. However, the sprung mass acceleration is increases, which reduces the comfort. Hence, optimal application of current has to be used to actuate MR damper for a given disturbance. Similarly, we also analyzed the system response of front and rear suspension system using the half-car model. We obtain the similar characteristics as that in quarter car model. To analyze the nonlinear system response of damper, we take a passive oil damper with cubic nonlinearity in spring and damping characteristics. We use half car model to study the influence of sinusoidal road excitation under the primary and secondary excitation for constant speed. The equilibrium analysis is carried out with method of multiple scales. The amplitude response curves versus frequency at the front and rear wheels are found. Primary resonance with 1:1 internal resonance between front and rear wheels is first studied. It shows the presence of the limit cycle over lower range of frequencies. Subsequently, due to the presence of cubic non-linearity in the system, we also perform nonlinear dynamical studies of half car model with 1:3 internal resonance condition. We obtain the system under the excitation near primary and superharmonic resonance and analyze the response at the front and rear wheels. Finally, we state that the linear and nonlinear study presented in the thesis can be used optimize the comfort performance of vehicle. The nonlinear analysis presented for passive oil damper can be extended to semi-active MR damper.

Contents

Chapter 1

Introduction

1.1 Motivation

The suspension system in automobiles is an area of active research in which many studies involving the control of linear and nonlinear characteristics dampers have been studied [1, 2, 4, 3]. Quarter car and half car models are widely used for studying the suspension system of automobiles [3, 2, 8]. Another interesting aspect is the application of control force to the suspension system using different control techniques [1, 2, 4]. In this thesis, we analyze the performance of semi-active and passive dampers subjected to different controlling and excitation forces, respectively.

1.2 Literature survey

Quarter car and half car models are widely used for studying the vehicle response assuming that the vehicle mass is acting at one wheel(quartet car) and two wheels(half car). For better passenger comfort the vibration amplitude need to be reduced using the suspension system. The suspension dampers are classified as passive, semi-active and active dampers. The semi-active and active dampers use control force to suppress the vibrations. Some of the semi-active dampers use MR(Magnetorheological) dampers to reduce the the vibrations. The active suspension with full feedback control and optimization with respect to ride comfort, working space of the suspension, road holding and control force of the suspension is studied by Hac [4] while the vehicle is traversing on random road surface. The vehicle performance characteristics are computed by solving Lyapunov and Riccati equations. The quarter car model with MR dampers is studied by Prabakar et al. [1]. The half car model with MR dampers at the front and rear wheels is studied by Prabakar et al.

[2] and they presented vehicle response curves. The rms values of state variables for the control force, suspension length and tyre deflection are computed using spectral decomposition methods by A.G.Thompson et al. [5]. An automobile is a nonlinear system because of the nonlinear properties of the components like suspension system, etc there can be chaos and bifurcations and hence half car model is studied by Zhu et al. [6] where the stiffness and damping are assumed to be nonlinear with displacement. It is observed by Zhu et al. [6] that the unstable region in frequency response diagram could lead to chaotic response and from the bifurcation diagram they concluded that the chaotic motion is sensitive to the damping value of the system. The full car nonlinear model is studied by Zhu et al. [7] where full vehicle is studied with the nonlinear stiffness and damping and they concluded that the chaotic vibration of the system could be avoided by having the frequency of excitation away from the unstable regions of the frequency response diagram.

The semi-active MR damper with the preview distance control is studied by Gopala Rao et al. [8] using spectral decomposition method and and they concluded that the overall performance improves with preview distance and has a limit after which the performance saturates. The random vibration of road vehicle using quarter car and half car models are studied by Bayrakdar [9] for finding the natural frequencies. Several idealized mechanical models for MR damper is studied by Spencer et al. [10] where in Bingham and Bouc-wen are studied along with other models and the proposed modified Bouc-wen is proved to be better than other methods in matching with the experimental results. So the modified Bouc-wen is followed in this report for characterizing the MR damper. The equivalent linearization of smooth hysteretic systems under random excitation is studied by Y.K.Wen [11] where in the hysteretic components satisfying non-linear differential equation are written in equivalent linear form to satisfy linear differential equation. The simulation of asymmetric hysteretic behaviour of material under tensile and compressive loading is studied using Bouc-wen model in Dobson et al. [12]. The shaping filter and sinusoidal approximation methods for generating random road profiles is discussed in F.Tyan et al. [13]. The skyhook, groundhook and hybrid configurations for quarter car suspension model are studied by Ahmadian et al. [14] where they studied the performance by varying the damping and the hybrid semi-active control is shown giving better performance. The experimental studies on quarter car suspension by Ahmadian et al. [15] showed that the transmissibility of sprung mass is reduced by skyhook and transmissibility of unsprung mass is reduced by groundhook control and the experiment is carried out using MR damper as an adjustable damper. The 2-DOF quarter car model with optimal preview control is studied by S.Narayanan et al. [16] where the preview of road irregularity is given as feed back to the active control system and the vehicle performance characteristics are significantly improved.

The stability and frequency analysis of quarter car model is carried out by Siewe [3] where one degree of freedom system is studied and they concluded that with the increasing force the periodic motion of the system becomes chaotic motion. The homoclinic bifurcation in quarter car model using Melnikov criterion is studided by Litak et al. [17] where they found critical Melnikov amplitude of the road surface profile above which the system show chaotic behaviour. The linear time delay active control in nonlinear quarter car model is studied by Naik et al. [18] where they used Melnikov technique to study onset of chaos from homoclinic bifurcation and concluded that there is effect of time-delay on the critical forces which lead to Melnikov chaos. They also concluded that the delayed feedback prevent the stable and unstable manifolds from tangling. Different methods to study the nonlinear systems and their stability are avalable [19, 20, 21]. The optimal control techniques are available in Anderson et al. [22].

The half car model with variable parameters is studied by Gao et al. [23] and they used Monte-Carlo simulation method to study the mean and standard deviation of vehicle natural frequencies and rms value of vehicle random response. The damping coefficient and stiffness coefficient effect on handling and comfort is studied by [24] and found that the damping has different coefficient values in compression and rebound. The influence of delay and parametric excitation on quarter car is studied by Koumene et al. [25]. The 1-1 internal resonance in a 2 degree of freedom oscillator was studied by Alexander [26] where the system is considered having cubic stiffness and linear damping and frequency response curves are shown having Hamiltonian Pitchfork bifurcation.

1.3 Outline of the thesis

Each chapter has mathematical formulation describing the formulation of the problem, experimental curve fitting and the vehicle response results. The mathematical model is taken from Prabakar et al. [1, 2] and the formulae are rederived. The experimental values are taken from Priyank [27] and curve fitting is performed to arrive at the damper characteristics. MR damper in quarter car model is dedicated to the quarter car with MR damper where the vehicle response curves are drawn for different currents. MR damper in half car model is dedicated to half car with MR dampers at the front and rear and vehicle response curves are shown for different currents at the front and rear. Nonlinear damper in half car model is dedicated to the half car model having nonlinear damper with cubic nonlinearity and amplitude response curves at front and rear are shown.

Chapter 2

MR damper in quarter car model

The MR damper is a semi-active suspension damper which is operated mainly by varying the current passed to it which in turn will vary the control force. This can be mathematically modeled using Bingham model, Bouc-Wen model and modified Bouc-Wen model which are compared by Spencer et al. [10]. Here we are following modified Bouc-Wen model and the nonlinear part is modeled using equivalent linearization mentioned by Wen [11]. The random road profile is modeled as white noise velocity satisfying covariance function. The state space equation will have the different states and the external excitation which will form as basis for the lyapunov equation. We solve the lyapunov equation by using lyap command in MATLAB control system tool box. We perform this process for different parameters obtained for different currents in MR damper and the analysis is presented.

2.1 Mathematical model

The standard 2-DOF quarter car model along with the parameters of MR damper is shown in the Fig. 2.1. In this present case, we characterize the MR damper using the modified Bouc-Wen model mentioned in Spencer et al. [10]. The equations of motion y_1 and y_2 corresponding to sprung mass M and unsprung mass m in the quarter car model can be found from Prabakar et al. [1] as

$$M\ddot{y_1} + K_s(y_1 - y_2) - (U)_{MR} = 0, \tag{2.1}$$

$$m\ddot{y_2} - K_s(y_1 - y_2) + K_t(y_2 - h) + (U)_{MR} = 0. \tag{2.2}$$

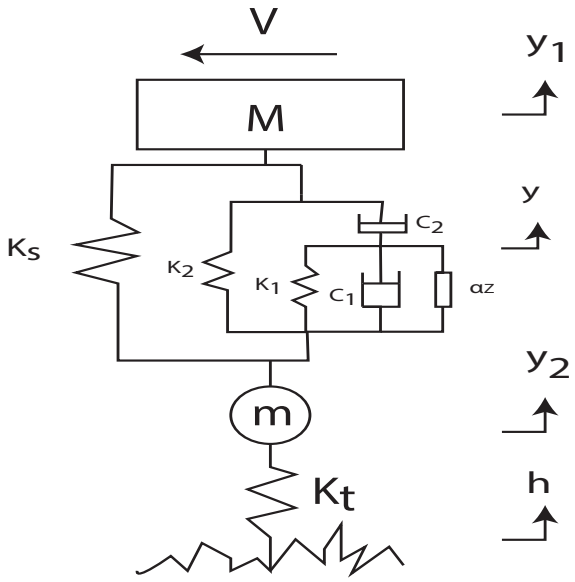

Figure 2.1: MR damper in quarter car model with modified Bouc-Wen model

where, K_s is stiffness, K_t is wheel stiffness, U_{MR} is control force and h is road height from ground. The control force U_{MR} can be written based on the modified Bouc-Wen model as

$$(U)_{MR} = K_2(y_2 - y_1) + C_2(\dot{y} - \dot{y_1}), \tag{2.3}$$

where, y is the pre-yielding displacement and it is governed by equation $\dot{y}$ which can can be obtained by equating the forces in C_2 with the combined forces in K_1, C_1, and αz as

$$\dot{y} = \frac{1}{C_1 + C_2}(K_1(y_2 - y_1) + C_1\dot{y_2} + C_2\dot{y_1} - \alpha z). \tag{2.4}$$

Here, z is the hysteretic displacements of the modified Bouc-Wen model which can be obtained from the equation given by Spencer et al. [10],

$$\dot{z} = -\gamma|\dot{y} - \dot{y_2}|z|z|^{(n-1)} - \beta(\dot{y} - \dot{y_2})|z|^n + A_1(\dot{y} - \dot{y_2}) \tag{2.5}$$

where, α, β, γ and A_1 are parameters of the modified Bouc-Wen model, K_1, K_2 are the stiffness values, C_1, C_2 are the damping coefficients and y_1, $\dot{y_1}$ are the displacement and velocity of the MR damper model, 'n' is the smoothness of transition from elastic to plastic response.

The equivalent linear form of the hysteretic displacement equation is available in [1] as,

$$\dot{z} = -C_h(\dot{y} - \dot{y_2}) - K_h z, \tag{2.6}$$

where, K_h and C_h values are mentioned in Prabakar et al. [28] and obtained by linearization technique mentioned in Wen [11]. This is calcuated by minimizing the mean square error,

$$C_h = \sqrt{\frac{2}{\pi}}[\gamma \frac{E[(\dot{y} - \dot{y_2})z]}{\sigma[(\dot{y} - \dot{y_2})]} + \beta\sigma[z]] - A_1 \tag{2.7}$$

$$K_h = \sqrt{\frac{2}{\pi}}[\beta \frac{E[(\dot{y} - \dot{y_2})z]}{\sigma[z]} + \gamma\sigma[(\dot{y} - \dot{y_2})]] \tag{2.8}$$

$$\sigma[z] = \sqrt{E[z^2]} \tag{2.9}$$

$$\sigma[\dot{y} - \dot{y_2}] = \sqrt{E[\dot{y}^2] - 2E[\dot{y}\dot{y_2}] + E[\dot{y_2}^2]} \tag{2.10}$$

$$\begin{aligned} E[\dot{y}^2] = \frac{1}{(C_1 + C_2)^2}[K_1^2(E[y_2^2] + E[y^2] - 2E[y_2 y]) \\ + C_1^2 E[\dot{y_2}^2] + C_2^2 E[\dot{y_1}^2] + \alpha_2 E[z_2] \\ + 2K_1 C_1(E[\dot{y_2} y_2] - E[\dot{y_2} y]) + 2C_1 C_2 E[\dot{y_1}\dot{y_2}] \\ - 2\alpha C_1 E[\dot{y_2} z] + 2K_1 C_2(E[\dot{y_1} y_2] \\ - E[\dot{y_1} y]) - 2\alpha K_1(E[y_2 z] - E[yz]) \\ - 2\alpha C_2 E[\dot{y_1} z]]. \end{aligned} \tag{2.11}$$

Equivalent linearization is used in obtaining the values C_h and K_h. Initial values of C_h and K_h are assumed and Lyapunov equation is solved to obtain the covariance values of the states and using these new values C_h and K_h are calculated and verified for convergence with previous C_h and K_h values and this procedure is repeated till the values converge to a predefined accuracy.

The random road profile model with white noise velocity derivation is available in [13] and the random road profile is satisfying the white noise velocity equation mentioned in [4, 1] as,

$$\dot{h(t)} + \alpha_r V h(t) = w(t) \tag{2.12}$$

where, $w(t)$ is a white noise process with covariance function $E[w(t)w^T(\tau)] = Q\delta(t - \tau)$ and Q is the spectral intensity given by $Q = 2\sigma^2\alpha_r V$, where σ^2 is the variance of the road profile, ω is the circular frequency and α_r is the road roughness coefficient and δ is dirac delta function.

The generated augmented state vector of a 2-DOF vehicle model using the equations of motion

for the MR suspension system is given by

$$\dot{X} = F_q X + Dw(t) \tag{2.13}$$

The individual matrices for F and D are available in the appendix and is also available in Prabakar et al. [1]. The state vector is given by X^T=[y_1 $\dot{y_1}$ y_2 $\dot{y_2}$ y z h].

The response of the system is obtained by solving matrix Lyapunov equation,

$$F_q P_q + P_q F_q^T + DQD^T = 0, \tag{2.14}$$

where, P represents the covariance matrix of the states. The performance characteristics are presented in terms of mean square values of sprung mass acceleration (J_1), suspension stroke(J_2), road holding parameter J_3 and control force J_4. These are calculated by full feedback control law given by Hac [4] and the control force used here will be for MR damper,

$$J_1 = \sum_{i=1}^{k}\sum_{j=1}^{k} F_q(2,i)F(2,j)P_q(i,j) \tag{2.15}$$

$$J_2 = P_q(1,1) - 2P_q(1,3) + P_q(3,3) \tag{2.16}$$

$$J_3 = P_q(3,3) - 2P_q(3,k) + P_q(k,k) \tag{2.17}$$

$$J_4 = E[U_{MR}^2] \tag{2.18}$$

where, number of state variables $k = 7$ for the modified Bouc-Wen model.

2.2 Experimental curve fitting

To analyze the performance of MR dampers subjected to different current, we use experiment results obtained by our group [27]. Fig. 2.2 shows typical characteristic graphs for a MR damper excited with an amplitude of 5 mm at a frequency of 1 Hz subjected to 0.5 A current. Subsequently, we obtain the parameters associated with the modified Bouc-Wen model by comparing the equations from the previous section with the experimental curves. Table 2.1 presents the corresponding parameters for different currents in MR damper.

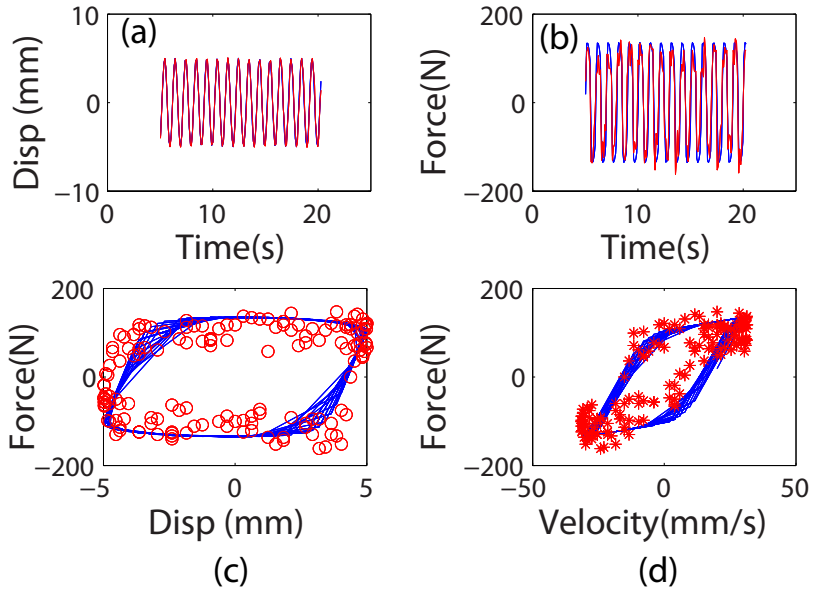

Figure 2.2: (a) The Displacement vs time, (b) force versus time, (c) force vs displacement and (d) force vs velocity

.

Table 2.1: MR damper parameters for different input current

Current Amp	K_1[N/m]	C_1[N-s/m]	K_2[N/m]	C_2[N-s/m]	α[N/m]	β $[m^{-2}]$	γ $[m^{-2}]$	A
0	100	800	120	80000	800	10000	3000	150
0.5	100	1000	120	80000	1000	10000	3000	150
1	100	2000	120	80000	2200	10000	3000	150
1.5	100	2200	120	80000	700	10000	3000	150

2.3 Vehicle performance curves

The vehicle performance curves for rms sprung mass acceleration, rms suspension stroke, rms road holding and rms control force are calculated for different input currents of the MR damper using the formulae mentioned in section 2.1.

The sprung mass acceleration of the vehicle shown in Fig. 2.3(a) is related to the comfort experienced by the passengers in the vehicle. If this value is high it means that the passengers will experience discomfort. So this value should be possible minimal value. When input current in the MR damper is increased we observed marginal increase in the sprung mass acceleration so it will be a limiting factor upto which we can increase the current in the MR damper. That means sprung mass acceleration limits the damping coefficient value that can be used in the suspension system. The suspension stroke shown in Fig. 2.3(b) is the length of the suspension system that can fit in the vehicle. If we have high value that means we should have bigger shock absorber. So it is required to have low suspension stroke to accommodate it in less space. We have observed that when we

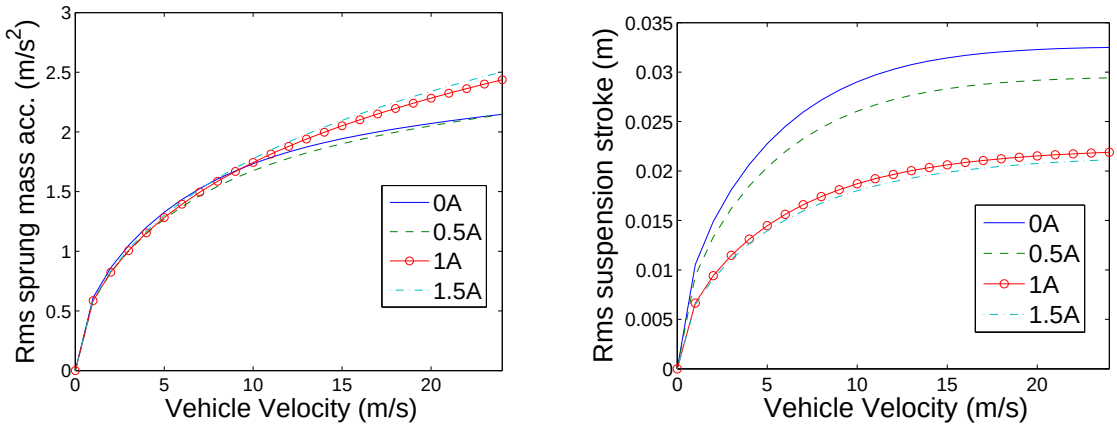

(a) (b)

Figure 2.3: (a) Variation of RMS sprung mass acceleration verses vehicle velocity and (b) RMS suspenion stroke verses vehicle velocity for different currents.

increased the current in the MR damper the suspension stroke is decreasing, so this is desirable effect.

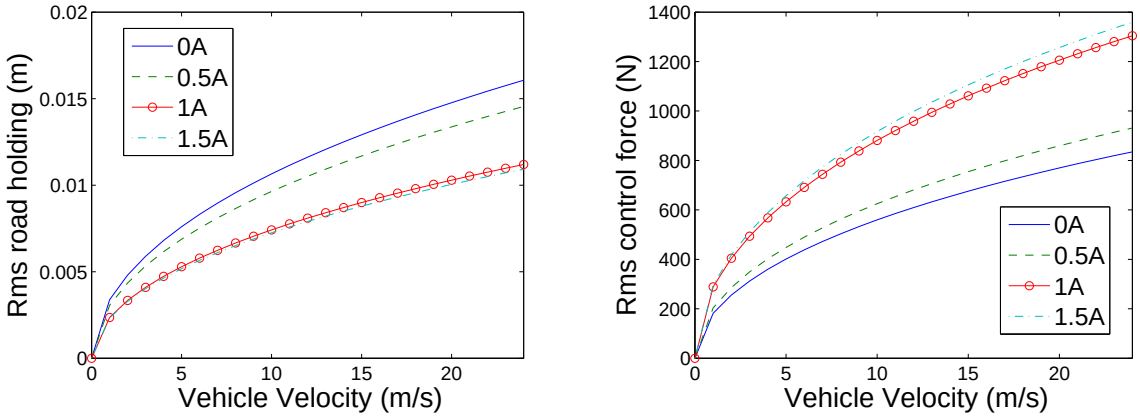

(a) (b)

Figure 2.4: Rms road holding and Rms control force for different currents

The road holding shown in Fig. 2.4a gives the vehicle handling and safety situation. This the distance by which the vehicle will be away from the road surface. So we need this value to be as minimal as possible to give better safety and handling. We have observed that when we increased the current in the MR damper the road holding is decreasing, so this is desirable effect. The control force shown in Fig. 2.4b is the force generated in the MR damper which will be used by the suspension system to negotiate with the road irregularity. We have observed that when we increased the current in the MR damper the control force is increasing, which is a desirable effect.

2.4 Summary

The quarter car model traveling on random road profile is modeled and the vehicle performance curves are drawn. We have obtained different parameters when different currents are passed to the MR damper in experiments conducted by our group [27]. When the performance curves are drawn we noticed that we should have a limiting current that be applied to the MR damper. This is because when we are increasing the current we will have desirable effects on suspension stroke, road holding and control force but there will be undesirable effect of sprung mass acceleration which is increasing making the discomfort for the passengers.

Chapter 3

MR damper in half car model

The MR damper in half car model is studied by Prabakar et al. [2]. There will be two MR dampers one at the front wheel and another at the rear wheel of the half car. We use similar approach mentioned in quarter car for the random road profile. We use state space formulation for performing the covariance analysis and solving the resulting lyapunov equation. We use the same characteristics mentioned in the previous section for the MR damper parameters for different currents. The two MR dampers are assumed to be having same characteristics.

3.1 Mathematical model

The half car model with MR dampers at the front and rear wheels is shown in the Fig. 3.1. The equation of motion can be derived using Lagrange equations. The equations of motion for the half car model suspension system with modified Bouc-Wen model are given in Prabakar et al. [2] as,

$$M\ddot{y_c} + K_f(y_c + a\theta - y_f) - (U_f)_{MR} + K_r(y_c - b\theta - y_r) - (U_r)_{MR} = 0 \tag{3.1}$$

$$I\ddot{\theta} + K_f(y_c + a\theta - y_f)a - a(U_f)_{MR} - K_r(y_c - b\theta - y_r)b + b(U_r)_{MR} = 0 \tag{3.2}$$

$$m_f\ddot{y_f} + K_{tf}(y_f - h_f) - K_f(y_c + a\theta - y_f) + (U_f)_{MR} = 0 \tag{3.3}$$

$$m_r\ddot{y_r} + K_{tr}(y_r - h_r) - K_r(y_c - b\theta - y_r) + (U_r)_{MR} = 0 \tag{3.4}$$

The control forces in modified Bouc-Wen model at the front wheel and rear wheel are given by,

$$(U_f)_{MR} = K_{2f}(y_f - y_c - a\theta) + C_{2f}(\dot{y_1}_f - \dot{y_c} - a\dot{\theta}) \tag{3.5}$$

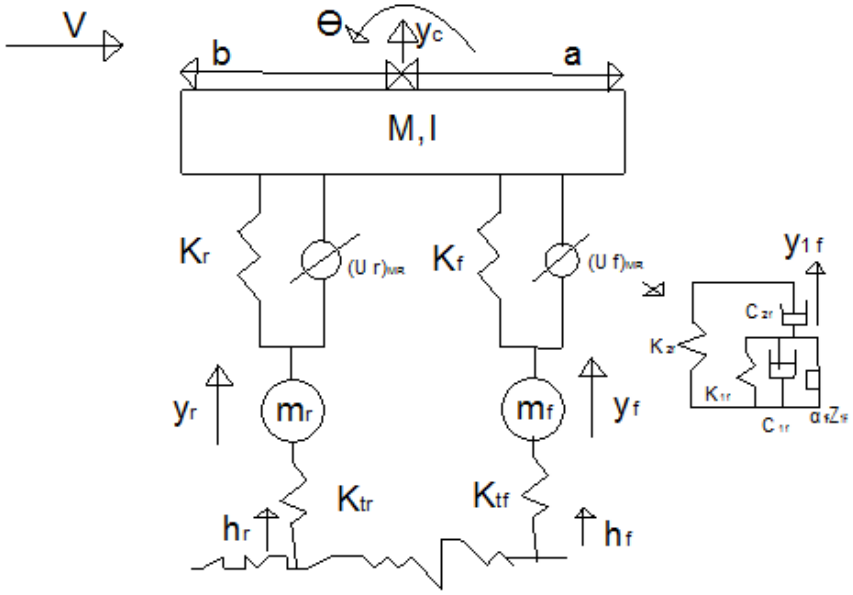

Figure 3.1: MR damper in half car with modified Bouc-Wen model

$$(U_r)_{MR} = K_{2r}(y_r - y_c + b\theta) + C_{2r}(\dot{y_{1r}} - \dot{y_c} + b\dot{\theta}) \tag{3.6}$$

One can obtain the $\dot{y_{1f}}$ by equating the forces in C_{2f} with combined forces in K_{1f}, C_{1f}, $\alpha_{1f}z_{1f}$ and similar calculation for rear MR damper.

$$\dot{y_{1f}} = \frac{1}{C_{1f} + C_{2f}}(K_{1f}(y_f - y_{1f}) + C_{1f}\dot{y_f} + C_{2f}\dot{y_c} + C_{2f}a\dot{\theta} - \alpha_{1f}z_{1f}) \tag{3.7}$$

$$\dot{y_{1r}} = \frac{1}{C_{1r} + C_{2r}}(K_{1r}(y_r - y_{1r}) + C_{1r}\dot{y_r} + C_{2r}\dot{y_c} - C_{2r}b\dot{\theta} - \alpha_{1r}z_{1r}) \tag{3.8}$$

where y_{1f}, y_{1r} are pre-yielding and z_{1f}, z_{1r} are hysteretic displacements of modified Bouc-Wen model. The hysteretic displacements are governed by modified Bouc-Wen model given by Spencer et al. [10],

$$\dot{z_{1f}} = -\gamma_{1f}|\dot{y_{1f}} - \dot{y_f}|z_{1f}|z_{1f}|^{(n-1)} - \beta_{1f}(\dot{y_{1f}} - \dot{y_f})|z_{1f}|^n + A_{1f}(\dot{y_{1f}} - \dot{y_f}) \tag{3.9}$$

$$\dot{z_{1r}} = -\gamma_{1r}|\dot{y_{1r}} - \dot{y_r}|z_{1r}|z_{1r}|^{(n-1)} - \beta_{1r}(\dot{y_{1r}} - \dot{y_r})|z_{1r}|^n + A_{1r}(\dot{y_{1r}} - \dot{y_r}) \tag{3.10}$$

where α_{1f}, β_{1f}, γ_{1f} and A_{1f} are parameters of the modified Bouc-Wen model, K_{1f}, K_{2f} are the stiffness, C_{1f}, C_{2f} are the damping coefficients and y_{1f}, $\dot{y_{1f}}$ are the displacement and velocity of the MR damper model, 'n' is the smoothness of transition from elastic to plastic response. And similar notations are taken for the suffix with 1r and 2r for the parameters in rear MR damper.

The equivalent linear form of the hysteretic displacement equations are given by

$$\dot{z_{1f}} = -C_{hf}(\dot{y_{1f}} - \dot{y_f}) - K_{hf} z_{1f} \tag{3.11}$$

$$\dot{z_{1r}} = -C_{hr}(\dot{y_{1r}} - \dot{y_r}) - K_{hr} z_{1r} \tag{3.12}$$

K_{hf}, C_{hf}, K_{hr}, C_{hr} are obtained by linearization technique [11] by minimizing the mean square error,

$$C_{hf} = \sqrt{\frac{2}{\pi}}[\gamma_{1f} \frac{E[(\dot{y_{1f}} - \dot{y_f}) z_{1f}]}{\sigma[(\dot{y_{1f}} - \dot{y_f})]} + \beta_{1f} \sigma[z_{1f}]] - A_{1f} \tag{3.13}$$

$$K_{hf} = \sqrt{\frac{2}{\pi}}[\beta_{1f} \frac{E[(\dot{y_{1f}} - \dot{y_f}) z_{1f}]}{\sigma[z_{1f}]} + \gamma_{1f} \sigma[(\dot{y_{1f}} - \dot{y_f})]] \tag{3.14}$$

$$C_{hr} = \sqrt{\frac{2}{\pi}}[\gamma_{1r} \frac{E[(\dot{y_{1r}} - \dot{y_r}) z_{1r}]}{\sigma[(\dot{y_{1r}} - \dot{y_r})]} + \beta_{1r} \sigma[z_{1r}]] - A_{1r} \tag{3.15}$$

$$K_{hr} = \sqrt{\frac{2}{\pi}}[\beta_{1r} \frac{E[(\dot{y_{1r}} - \dot{y_r}) z_{1r}]}{\sigma[z_{1r}]} + \gamma_{1r} \sigma[(\dot{y_{1r}} - \dot{y_r})]] \tag{3.16}$$

Equivalent linearization is used in obtaining the values of C_{hf}, K_{hf}, C_{hr} and K_{hr}. Similar procedure mentioned for quarter car model is followed for the evaluation of these values.

The random road profile is taken to be similar to the one mentioned in Prabakar et al. [28] as

$$\dot{h_1}(t) + \alpha_r V h_1(t) = w(t) \tag{3.17}$$

$$\dot{h_2}(t) + \alpha_r V h_2(t) = w(t - t_2) \tag{3.18}$$

where h_1, h_2 are the road height at the front wheel and rear wheel, V is velocity of the vehicle and $w(t)$ is the white noise process following covariance function.

The state vector of a half car model using the equations of motion for the MR suspension system is given by

$$\dot{X}_a = F_h X_a + D_1 w(t) + D_2 w(t - t_2) \tag{3.19}$$

The individual matrices for F_h, D_1 and D_2 are available in appendix and also in Prabakar et al. [2] and X_a^T=[y_c $\dot{y_c}$ θ $\dot{\theta}$ y_f $\dot{y_f}$ y_r $\dot{y_r}$ y_{1f} z_{1f} y_{1r} z_{1r} h_f h_r].

The response of the system is obtained by solving matrix Lyapunov equation,

$$F_h P_h + P_h F_h^T + D_1 Q D_1^T + D_2 Q D_2^T + \phi(t, t_2) D_1 Q D_2^T + D_2 Q D_1^T \phi(t, t_2)^T = 0 \tag{3.20}$$

where P_h represents the covariance matrix of the states. And $\phi(t, t_2) = e^{F_h*(t-t_2)}$ is the state transition matrix, here the time lag is assumed to be minimal so the state transition matrix can be identity matrix. The rms values of the vehicle performance characteristics are obtained by taking the square root of the values of $J1_h$(Sprung mass acceleration), $J2_h$(Front suspension stroke front), $J3_h$(Road holding front), $J4_h$(Pitch acceleration), $J5_h$(Rear suspension stroke), $J6_h$(Rear road holding), $J7_h$(Front control force) and $J8_h$(Rear control force).

$J1_h = c1 * P_h * c1^T$,

$J2_h = c2 * P_h * c2^T$,

$J3_h = c3 * P_h * c3^T$,

$J4_h = c4 * P_h * c4^T$,

$J5_h = c5 * P_h * c5^T$,

$J6_h = c6 * P_h * c6^T$,

$J7_h = c7 * P_h * c7^T$ and

$J8_h = c8 * P_h * c8^T$

where

$c1 = F_h(2, :)$,

c2=[1 0 a 0 -1 0 0 0 0 0 0 0 0 0],

c3=[0 0 0 0 1 0 0 0 0 0 0 0 -1 0],

$c4 = F_h(4, :)$,

c5=[1 0 -b 0 0 0 -1 0 0 0 0 0 0 0],

c6=[0 0 0 0 0 0 1 0 0 0 0 0 0 -1],

$c7 = [-K_{2f} \ -C_{2f}+\frac{C_{2f}^2}{C_{1f}+C_{2f}} \ -aK_{2f} \ -aC_{2f}+\frac{aC_{2f}^2}{C_{1f}+C_{2f}} \ K_{2f}+\frac{K_{1f}C_{2f}}{C_{1f}+C_{2f}} \ \frac{C_{1f}C_{2f}}{C_{1f}+C_{2f}} \ 0 \ 0 \ \frac{-K_{1f}C_{2f}}{C_{1f}+C_{2f}} \ \frac{-\alpha_{1f}C_{2f}}{C_{1f}+C_{2f}} \ 0 \ 0 \ 0 \ 0]$

$c8 = [-K_{2r} \ -C_{2r}+\frac{C_{2r}^2}{C_{1r}+C_{2r}} \ -aK_{2r} \ -aC_{2r}+\frac{aC_{2r}^2}{C_{1r}+C_{2r}} \ K_{2r}+\frac{K_{1r}C_{2r}}{C_{1r}+C_{2r}} \ \frac{C_{1r}C_{2r}}{C_{1r}+C_{2r}} \ 0 \ 0 \ \frac{-K_{1r}C_{2r}}{C_{1r}+C_{2r}} \ \frac{-\alpha_{1r}C_{2r}}{C_{1r}+C_{2r}} \ 0 \ 0 \ 0 \ 0]$.

3.2 Experimental curve fitting

The same parameters mentioned in the section 2.2 are used for half car model. The same parameters are used at the front wheel and rear wheel.

3.3 Vehicle performance curves

The vehicle performance curves for rms sprung mass acceleration, rms pitch acceleration, rms suspension stroke front, rms suspension stroke rear, rms road holding front, rms road holding rear, rms

control force front and rms control force rear are calculated for different input currents of the MR damper. The time lag between front and rear wheels is neglected for calculating the vehicle response curves.

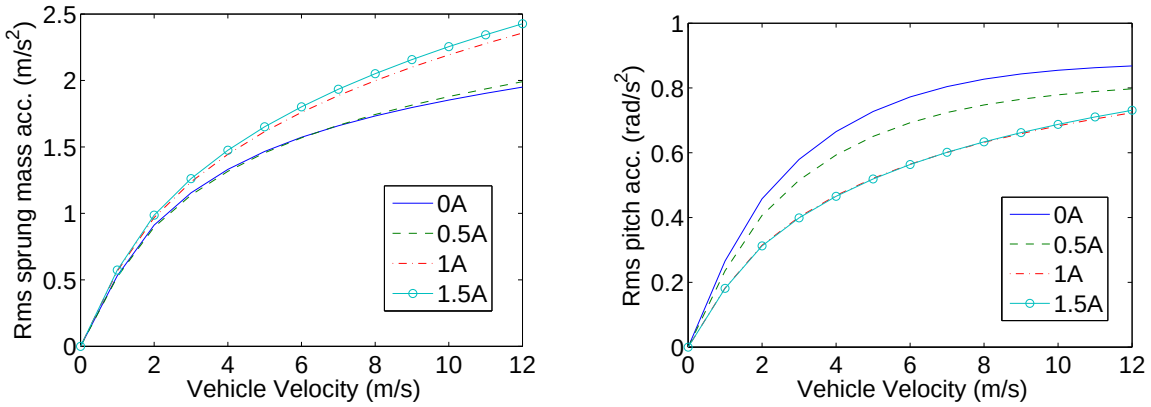

(a) (b)

Figure 3.2: Rms sprung mass and pitch acceleration for different currents

From the above Fig. 3.2(a) we can conclude that the sprung mass acceleration is increasing with the increasing input current. This is not desirable as this will limit the maximum input current we can supply to the MR damper. The increase in sprung mass acceleration reduces the comfort for the passengers in the vehicle. It is observed from above Fig. 3.2(b) that the pitch acceleration is decreasing with the increasing current in MR damper. This is desirable effect which will improve the comfort for the passengers in the vehicle.

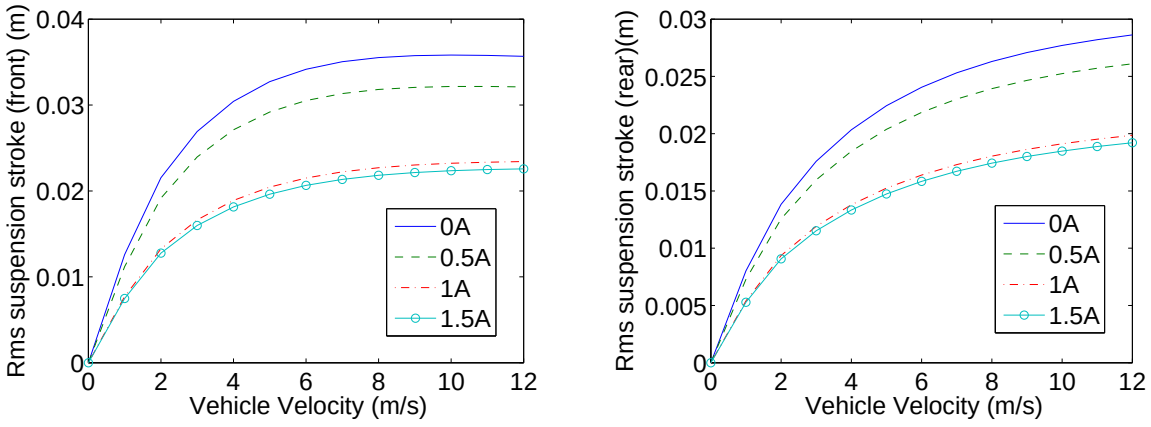

(a) (b)

Figure 3.3: Rms suspension stroke at front and rear for different currents

From the Fig. 3.3(a) on front suspension stroke it is observed that the front suspension stroke is decreasing with the increasing current in MR damper. This is desirable effect which will reduce

suspension space requirements at the front wheel of the vehicle. It is observed from the Fig. 3.3(b) on rear suspension stroke that the rear suspension stroke is decreasing with the increasing current in MR damper. This is desirable effect which will reduce suspension space requirements at the rear wheel of the vehicle.

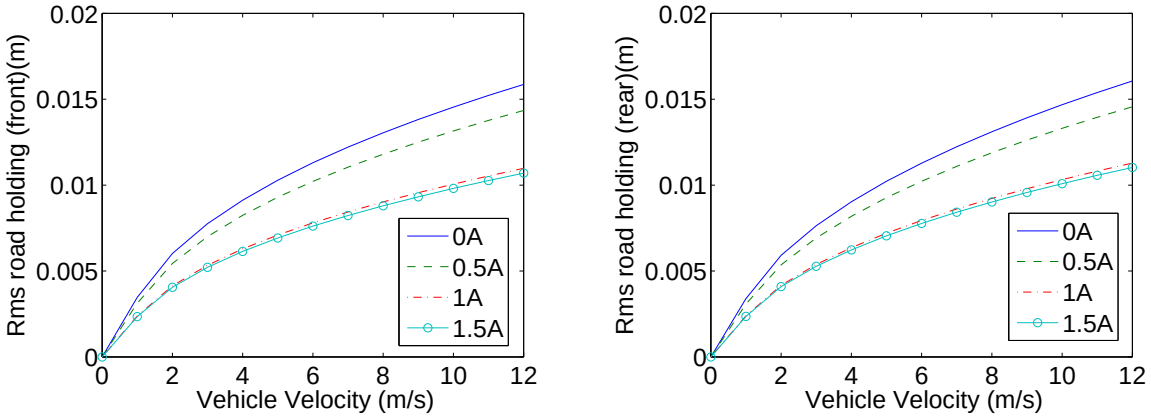

(a) (b)

Figure 3.4: Rms road holding at front and rear for different currents

We can conclude from the road holding Figs. 3.4(a) and 3.4(b) that the front road holding is decreasing with the increasing current in MR damper. This is desirable effect which will improve the safety and handling of the vehicle at the front wheel. It is observed that the rear road holding is decreasing with the increasing current in MR damper. This is desirable effect which will improve the safety and handling of the vehicle at the rear wheel.

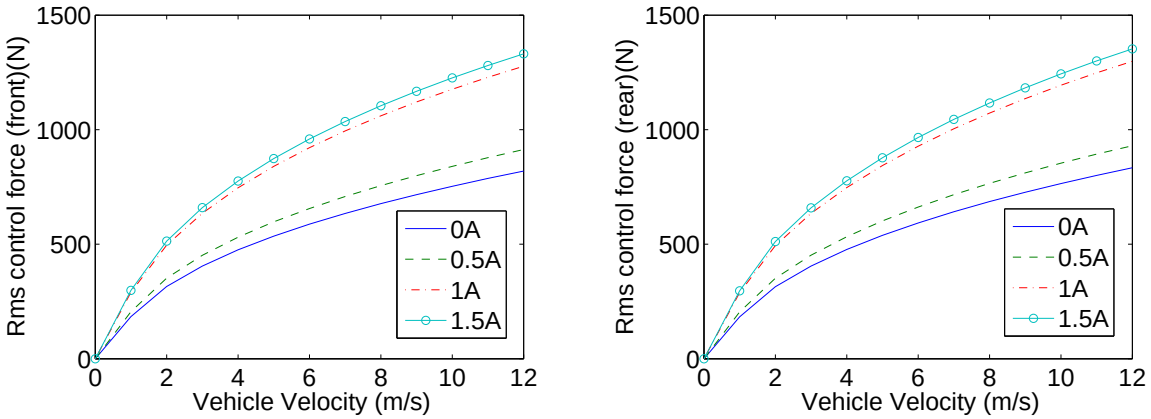

(a) (b)

Figure 3.5: Rms control force at front and rear for different currents

From the control force Figs. 3.5(a) and 3.5(b) it is observed that the front control force is

increasing with the increasing current in MR damper. This is desirable effect which will improve the other parameters of the vehicle at the front wheel. There will be some limit to the control force after which the sprung mass acceleration can not be increased beyond a certain value. We can also observe that the rear control force is increasing with the increasing current in MR damper. This is desirable effect which will improve the other parameters of the vehicle at the rear wheel. There will be some limit to the control force after which the sprung mass acceleration can not be increased beyond a certain value.

3.4 Summary

The half car model traveling on random road profile is modeled and the vehicle performance curves are drawn. We have used same parameters used in previous section which are obtained in experiments conducted by our group [27]. When the performance curves are drawn we noticed that we have similar effects at the front wheel and rear wheel. And there is some limiting current that can be applied to the MR damper. This is because when we are increasing the current we will have desirable effects on suspension stroke (at front wheel and rear wheel), road holding(at front wheel and rear wheel) and control force(at front wheel and rear wheel) but there will be undesirable effect of sprung mass acceleration which is increasing making the discomfort for the passengers.

Chapter 4

Nonlinear passive damper in half car model

In this section we consider vehicle having stiffness and damper with cubic nonlinearity and the vehicle is travelling on sinusoidal road surface with constant velocity. We have 2 scenarios considered for this model. In the first scenario the effects of oscillations of the front and rear sprung mass are assumed to have 1-1 internal resonance (a=b in the fig. 4.1). In this scenario we have primary resonance for the sprung mass at the front and rear part of the vehicle. In the second case we consider a and b are not equal and we assume that there is 1-3 internal resonance between the masses at front and rear part of the vehicle. In this case we present the primary and subharmonic resonances. We use method of multiple scales for arriving at the envelope equations and these equations are used to arrive at the equilibrium curves. In this thesis the equilibrium curves show the amplitude vs frequency response. These curves give and indication at what frequency there is resonance amplitude and the force at which there is steady state solution beyond which there will be onset of unsteady behaviour.

4.1 Mathematical model for 1:1 internal resonance

The schematic diagram of half car suspension is shown in the Fig. 4.1. The half car with sprung mass M, moment of inertia I and a, b are the distances to the front and rear edge of the sprung mass from the center of gravity. The vehicle is assumed to travel with a constant velocity V. K_{1r},K_{1f} are the stiffness values and F_{hr}, F_{hf} are the nonlinear damping forces with cubic nonlinearity for the stiffness and damping. z_1, z_2 are the two degrees of freedom and they are calculated from pitch

angle θ and heave motion y_c. The equation of motion for the half car can be derived using Newton's

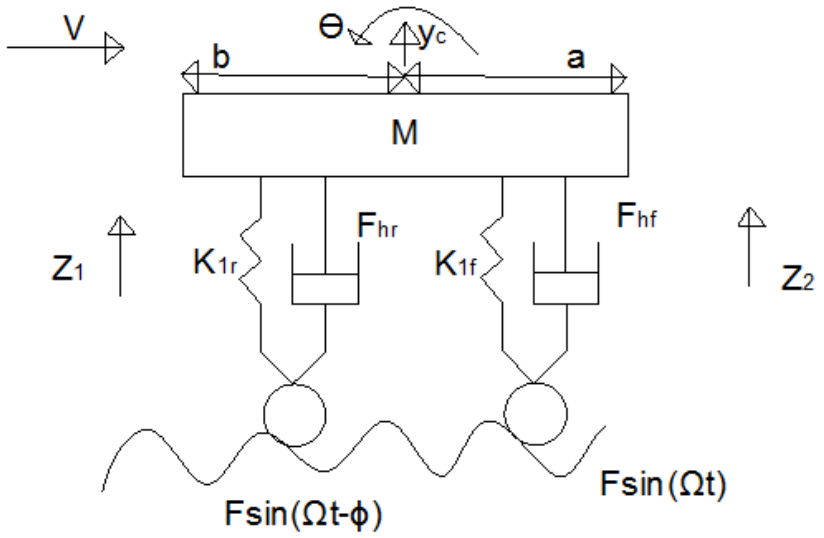

Figure 4.1: Halfcar model with periodic excitation

laws.

$$M\ddot{y_c} + K_{1f}z_1 + F_{hf} + K_{1r}z_2 + F_{hr} = 0 \tag{4.1}$$

$$I\ddot{\theta} + aK_{1f}z_1 + aF_{hf} - bK_{1r}z_2 - bF_{hr} = 0 \tag{4.2}$$

where $F = A\Omega^2$, $y_f = A\sin(\Omega t)$, $y_r = A\sin(\Omega t - \phi)$, $z_1 = y_c + a\theta - y_f$, $z_2 = y_c - b\theta - y_r$, $F_{hf} = K_{2f}{z_1}^3 + C_{1f}\dot{z_1} + C_{2f}\dot{z_1}^3$, $F_{hr} = K_{2r}{z_2}^3 + C_{1r}\dot{z_2} + C_{2r}\dot{z_2}^3$. The above equations in $\ddot{y_c}$, $\ddot{\theta}$ can be converted into equations in $\ddot{z_1}$, $\ddot{z_2}$. And we can make the equations in non dimensional form by dividing the equations with ${\omega_1}^2$ where we substitute $\omega_1 t = \tau$ and $\Omega^{'} = \frac{\Omega}{\omega_1}$.

$$\ddot{z_1} + z_1 + B_1{z_1}^3 + B_2\dot{z_1} + B_3\dot{z_1}^3 + B_4z_2 + B_5{z_2}^3 + B_6\dot{z_2} + B_7\dot{z_2}^3 = A{\Omega^{'}}^2\sin(\Omega^{'}\tau) \tag{4.3}$$

$$\ddot{z_2} + \frac{{\omega_2}^2}{{\omega_1}^2}z_2 + B_8z_1 + B_9{z_1}^3 + B_{10}\dot{z_1} + B_{11}\dot{z_1}^3 + B_{12}{z_2}^3 + B_{13}\dot{z_2} + B_{14}\dot{z_2}^3 = A{\Omega^{'}}^2\sin(\Omega^{'}\tau - \phi) \tag{4.4}$$

where, ${\omega_1}^2 = (\frac{1}{M} + \frac{a^2}{I})K_{1f}$, $B_1 = (\frac{1}{M} + \frac{a^2}{I})\frac{K_{2f}}{{\omega_1}^2}$, $B_2 = (\frac{1}{M} + \frac{a^2}{I})\frac{C_{1f}}{\omega_1}$, $B_3 = (\frac{1}{M} + \frac{a^2}{I})C_{2f}\omega_1$, $B_4 = (\frac{1}{M} - \frac{ab}{I})\frac{K_{1r}}{{\omega_1}^2}$, $B_5 = (\frac{1}{M} - \frac{ab}{I})\frac{K_{2r}}{{\omega_1}^2}$, $B_6 = (\frac{1}{M} - \frac{ab}{I})\frac{C_{1r}}{\omega_1}$, $B_7 = (\frac{1}{M} - \frac{ab}{I})C_{2r}\omega_1$, ${\omega_2}^2 = (\frac{1}{M} + \frac{b^2}{I})K_{1r}$, $B_8 = (\frac{1}{M} - \frac{ab}{I})\frac{K_{1f}}{{\omega_1}^2}$, $B_9 = (\frac{1}{M} - \frac{ab}{I})\frac{K_{2f}}{{\omega_1}^2}$, $B_{10} = (\frac{1}{M} - \frac{ab}{I})\frac{C_{1f}}{\omega_1}$, $B_{11} = (\frac{1}{M} - \frac{ab}{I})C_{2f}\omega_1$, $B_{12} = (\frac{1}{M} + \frac{b^2}{I})\frac{K_{2r}}{{\omega_1}^2}$, $B_{13} = (\frac{1}{M} + \frac{b^2}{I})\frac{C_{1r}}{\omega_1}$, $B_{14} = (\frac{1}{M} + \frac{b^2}{I})C_{2r}\omega_1$. The solution to the equations (4.3) and

(4.4) can be written in method of multiple scales.

$$z_1 = z_{10}(T_0, T_1) + \epsilon z_{11}(T_0, T_1) + O(\epsilon^2)$$
$$z_2 = z_{20}(T_0, T_1) + \epsilon z_{21}(T_0, T_1) + O(\epsilon^2) \tag{4.5}$$

where z_{10}, z_{11}, z_{20}, z_{21} are functions to be determined, $T_0 = t$, $T_1 = \epsilon t$, $T_n = \epsilon^n t$. The differential operators become

$$\frac{d}{dt} = D_0 + \epsilon D_1 + ...$$
$$\frac{d^2}{dt^2} = {D_0}^2 + \epsilon D_0 D_1 + \epsilon^2({D_1}^2 + 2D_0 D_2) + ... \tag{4.6}$$

The primary resonance is studied when the front and rear wheel sprung masses have same natural frequencies that is when a and b are equal (when the center of gravity of the sprung mass is at the geometric center). To determine the amplitude of oscillation at primary resonance the force term and the nonlinear terms are assumed to be smaller so they are ordered with ϵ. Equating the coefficients of the like powers of ϵ gives the following differential equations.

$${D_0}^2 z_{10} + {\omega_1}^2 z_{10} = 0$$
$${D_0}^2 z_{20} + {\omega_2}^2 z_{20} = 0 \tag{4.7}$$

$$\begin{aligned} {D_0}^2 z_{11} + z_{11} = -2D_0 D_1 z_{10} - B_1 {z_{10}}^3 - B_2 D_0 z_{10} - B_3 (D_0 z_{10})^3 - B_4 z_{20} \\ -B_5 {z_{20}}^3 - B_6 D_0 z_{20} - B_7 D_0 {z_{20}}^3 + F\sin(\Omega^{'}\tau) \\ {D_0}^2 z_{21} + (\frac{{\omega_2}^2}{{\omega_1}^2}) z_{21} = -2D_0 D_1 z_{20} - B_8 z_{10} - B_9 {z_{10}}^3 - B_{10} D_0 z_{10} - B_{11} (D_0 z_{10})^3 \\ -B_{12} {z_{20}}^3 - B_{13} D_0 z_{20} - B_1 4 (D_0 z_{20})^3 + F\sin(\Omega^{'}\tau - \phi) \end{aligned} \tag{4.8}$$

The general solution to equation 4.7 gives

$$z_{10} = A_1(T_1) e^{i\omega_1 T_0} + \bar{A_1}(T_1) e^{-i\omega_1 T_0}$$
$$z_{20} = A_2(T_1) e^{i\omega_2 T_0} + \bar{A_2}(T_1) e^{-i\omega_2 T_0} \tag{4.9}$$

Substituting equation 4.9 into equation 4.8 and collecting the secular terms with the conditions $\omega_1 = 1$, $\Omega^{'} = \omega_1 + \epsilon\sigma$ and $\omega_1 = \omega_2$ and equating the real and imaginary parts to zero gives the

following envelope equations for primary resonance at front wheel with internal resonance at rear wheel. Here we substitute $A_m = \frac{1}{2}a_m e^{i\theta_m}$. The ϕ is calculated using the time taken for the vehicle to travel its length of 2.5m using 10m/s speed.

$$a_1^{'} = \frac{B_2 a_1}{2} + \frac{3B_3 a_1^3 \omega_1^2}{8} + \frac{B_4 a_2 \sin(\gamma_2)}{2\omega_1} + \frac{3B_5 a_2^3 \sin(\gamma_2)}{8\omega_1} + \frac{B_6 a_2 \omega_2 \cos(\gamma_2)}{2\omega_1} + \frac{3B_7 a_2^3 \omega_2^3 \cos(\gamma_2)}{8\omega_1} + \frac{F\cos(\gamma_1)}{2\omega_1} \tag{4.10}$$

$$\gamma_1^{'} = \sigma - \frac{3B_1 {a_1}^3}{8a_1\omega_1} - \frac{B_4 a_2 \cos(\gamma_2)}{2a_1\omega_1} - \frac{3B_5 a_2^3 \cos(\gamma_2)}{8a_1\omega_1} + \frac{B_6 a_2 \omega_2 \sin(\gamma_2)}{2a_1\omega_1} + \frac{3B_7 a_2^3 \omega_2^3 \sin(\gamma_2)}{8a_1\omega_1} + \frac{F\sin(\gamma_1)}{2a_1\omega_1} \tag{4.11}$$

$$a_2^{'} = \frac{B_8 a_1 \sin(\gamma_2)}{2\omega_2} + \frac{3B_9 a_1^3 \sin(\gamma_2)}{8\omega_2} - \frac{B_{10} a_1 \omega_1 \cos(\gamma_2)}{2\omega_2} - \frac{3B_{11} a_1^3 \omega_1^3 \cos(\gamma_2)}{8\omega_2} - \frac{B_{13} a_2 \omega_2}{2\omega_2} - \frac{3B_{14} a_2^3 \omega_2^3}{8\omega_2} - \frac{F\cos(\gamma_1 - \gamma_2 - \Omega\phi)}{2\omega_2} \tag{4.12}$$

$$\gamma_2^{'} = \frac{B_8 a_1 \cos(\gamma_2)}{2a_2\omega_2} + \frac{3B_9 a_1^3 \cos(\gamma_2)}{8a_2\omega_2} + \frac{B_{10} a_1 \omega_1 \sin(\gamma_2)}{2a_2\omega_2} + \frac{3B_{11} a_1^3 \omega_1^3 \sin(\gamma_2)}{8a_2\omega_2} + \frac{3B_{12} a_2^3}{8a_2\omega_2} - \frac{F\sin(\gamma_1 - \gamma_2 - \Omega\phi)}{2a_2\omega_2} \tag{4.13, 4.14}$$

where $\gamma_1 = \sigma - \theta_1$ and $\gamma_2 = \theta_2 - \theta_1$.

4.2 Mathematical model for 1:3 internal resonance

In this section we consider that there will be 1:3 internal resonance between the front and rear portions of the sprung mass. This may happen because of differential stiffness values at the front and rear wheels. The similar procedure is followed as mentioned earlier but we need to have a condition that the natural frequency at the rear is 3 times that of the front portion of the mass.

4.2.1 Primary resonance

Substituting equation (4.9) into equation (4.8) and collecting the secular terms with the conditions $\omega_1 = 1$, $\Omega^{'} = \omega_1 + \epsilon\sigma_1$ and $3\omega_1 = \omega_2 - \epsilon\sigma_2$ and equating the real and imaginary parts to zero gives the following envelope equations for primary resonance at front wheel with internal resonance at rear wheel. Here we substitute $A_m = \frac{1}{2}a_m e^{i\theta_m}$. The ϕ is calculated using the time taken for the

vehicle to travel its length of 2.5m using 10m/s speed.

$$
\begin{aligned}
a_1^{'} &= -\frac{B_2 a_1}{2} - \frac{3B_3 a_1^3}{8} - \frac{F\cos(\gamma_1)}{2} \\
\gamma_1^{'} &= \sigma_1 - \frac{3B_1 {a_1}^2}{8} + \frac{F\sin(\gamma_1)}{a_1} \\
a_2^{'} &= -\frac{B_9 a_1^3 \sin(\gamma_2)}{24} - \frac{B_{11} a_1^3 \cos(\gamma_2)}{24} - \frac{B_{13} a_2}{2} - \frac{27 B_{14} a_2^3}{8} \\
\gamma_2^{'} &= -\sigma_2 + \frac{9B_1 {a_1}^2}{8} - \frac{F\sin(\gamma_1)}{2a_1} - \frac{B_9 a_1^3 \cos(\gamma_2)}{24a_2} + \frac{B_{11} a_1^3 \sin(\gamma_2)}{24a_2} - \frac{3B_{12} a_2^3}{24a_2}
\end{aligned} \tag{4.15}
$$

where $\gamma_1 = \sigma_1 T_1 - \theta_1$ and $\gamma_2 = -\sigma_2 T_1 + 3\theta_1 - \theta_2$.

4.2.2 Superharmonic resonance

Now including the forcing term in the equation (4.9) gives the below equations,

$$
\begin{aligned}
{D_0}^2 z_{10} + {\omega_1}^2 z_{10} &= F\sin(\Omega^{'}\tau) \\
{D_0}^2 z_{20} + {\omega_2}^2 z_{20} &= F\sin(\Omega^{'}\tau - \phi)
\end{aligned} \tag{4.16}
$$

$$
\begin{aligned}
{D_0}^2 z_{11} + z_{11} &= -2D_0 D_1 z_{10} - B_1 {z_{10}}^3 - B_2 D_0 z_{10} - B_3 (D_0 z_{10})^3 - B_4 z_{20} \\
&\quad -B_5 {z_{20}}^3 - B_6 D_0 z_{20} - B_7 D_0 {z_{20}}^3 \\
{D_0}^2 z_{21} + (\frac{{\omega_2}^2}{{\omega_1}^2}) z_{21} &= -2D_0 D_1 z_{20} - B_8 z_{10} - B_9 {z_{10}}^3 - B_{10} D_0 z_{10} - B_{11} (D_0 z_{10})^3 \\
&\quad -B_{12} {z_{20}}^3 - B_{13} D_0 z_{20} - B_1 4 (D_0 z_{20})^3
\end{aligned} \tag{4.17}
$$

The general solution to equation (4.16) gives,

$$
\begin{aligned}
z_{10} &= A_1(T_1) e^{i\omega_1 T_0} + \bar{A_1}(T_1) e^{-i\omega_1 T_0} + \frac{F e^{i(\Omega T_0 - \frac{\pi}{2})}}{2({\omega_1}^2 - {\Omega'}^2)} - \frac{F e^{-i(\Omega T_0 + \frac{\pi}{2})}}{2({\omega_1}^2 - {\Omega'}^2)} \\
z_{20} &= A_2(T_1) e^{i\omega_2 T_0} + \bar{A_2}(T_1) e^{-i\omega_2 T_0} + \frac{F e^{i(\Omega T_0 - \phi - \frac{\pi}{2})}}{2({\omega_2}^2 - {\Omega'}^2)} - \frac{F e^{-i(\Omega T_0 - \phi + \frac{\pi}{2})}}{2({\omega_2}^2 - {\Omega'}^2)}
\end{aligned} \tag{4.18}
$$

Substituting equation (4.18) into equation (4.17) and collecting the secular terms with the conditions $\omega_1 = 1{,}3\Omega^{'} = \omega_1 + \epsilon\sigma_1$ and $3\omega_1 = \omega_2 + \epsilon\sigma_2$ and equating the real and imaginary parts to zero gives the following envelope equations for superharmonic resonance at front wheel with internal resonance

at rear wheel.

$$
\begin{aligned}
a_1^{'} &= -B_1 B_{111}^3 \cos(\gamma_1) - \frac{B_2 a_1}{2} - \frac{3B_3 a_1^3}{8} - 3B_3 B_{111}^2 \Omega^{'2} a_1 - B_3 B_{111}^3 \Omega^{'3} \sin(\gamma_1) \\
&\quad - B_5 B_{111}^3 \cos(\gamma_1 - 3\phi) - B_7 B_{111}^3 \Omega^{'3} \sin(\gamma_1 - 3\phi) \\
\gamma_1^{'} &= \sigma_1 - \frac{3B_1 a_1^2}{8} - 3B_1 B_{111}^2 + \frac{B_1 B_{111}^3 \sin(\gamma_1)}{a_1} - \frac{B_3 B_{111}^3 \Omega^{'3} \cos(\gamma_1)}{a_1} \\
&\quad + \frac{B_5 B_{111}^3 \sin(\gamma_1 - 3\phi)}{a_1} - \frac{B_7 B_{111}^3 \Omega^{'3} \cos(\gamma_1 - 3\phi)}{a_1} \\
a_2^{'} &= \frac{-B_9 a_1^3 \sin(\gamma_2)}{24} + \frac{B_{11} a_1^3 \cos(\gamma_2)}{24} - \frac{B_{13} a_2}{2} - \frac{27 B_{14} a_2^3}{8} - 3B_{14} B_{222}^2 \Omega^{'2} a_2 \\
\gamma_2^{'} &= \sigma_2 + \frac{9B_1 a_1^2}{8} + 9B_1 B_{111}^2 - \frac{3B_1 B_{111}^3 \sin(\gamma_1)}{a_1} + \frac{3B_3 B_{111}^3 \Omega^{'3} \cos(\gamma_1)}{a_1} \\
&\quad - \frac{3B_5 B_{111}^3 \sin(\gamma_1 - 3\phi)}{a_1} + \frac{3B_7 B_{111}^3 \Omega^{'3} \cos(\gamma_1 - 3\phi)}{a_1} - \frac{-B_9 a_1^3 \cos(\gamma_2)}{24 a_2} \\
&\quad - \frac{B_{11} a_1^3 \sin(\gamma_2)}{24} - \frac{B_{12} a_2^3}{8 a_2} - B_{12} B_{222}^2 a_2
\end{aligned} \tag{4.19}
$$

where $\gamma_1 = \sigma_1 T_1 - \theta_1$, $\gamma_2 = \sigma_2 T_1 + 3\theta_1 - \theta_2$, $B_{111} = \frac{F}{2(\omega_1^2 - \Omega^2)}$ and $B_{222} = \frac{F}{2(\omega_2^2 - \Omega^2)}$.

4.3 Experimental curve fitting

Using the experimental values from the experiment conducted by our group [27], the curve fitting is performed and the fig. 4.2 shows the corresponding curves. The following values are found from the

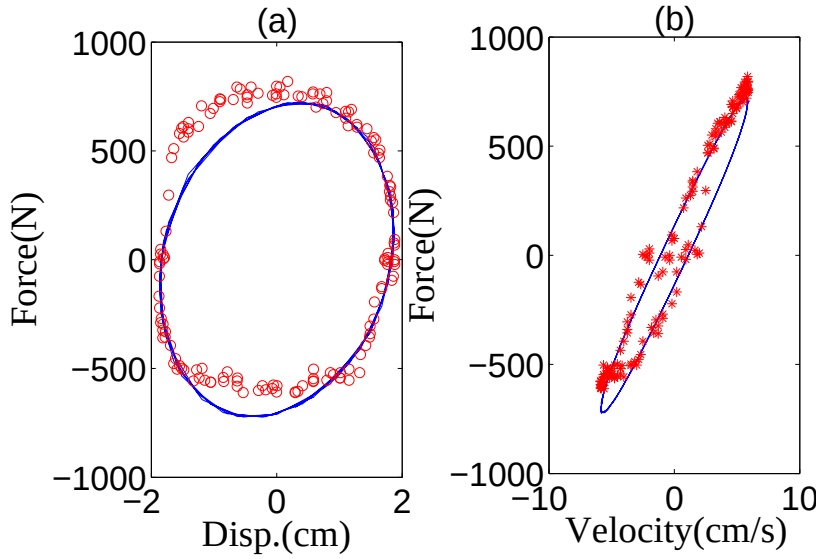

Figure 4.2: (a) Force versus displacement (b) Force versus velocity

curve fitting and these are appropriate for further analysis by using them in the envelope equations.

The parameters for the oil damper are found as $K_1 = 9000$ N/m, $K_2 = -5000$ kN/m^3, $C_1 = 12000$ Ns/m, $C_2 = -4000$ Ns^3/m^3.

4.4 Frequency response results for 1:1 internal resonance

The parameter values used in evaluation of the above envelope equations are $K_{1f} = 9000N/m$, $K_{1r} = 9000N/m$, $K_{2f} = -5000kN/m^3$, $K_{2r} = -5000kN/m^3$, $C_{1f} = 12000Ns/m$, $C_{1r} = 12000Ns/m$, $C_{2f} = -4000Ns^3/m^3$, $C_{2r} = -4000Ns^3/m^3$, $F = 0.008$ and $\epsilon << 1$. The vehicle is assumed to travel at a speed of $10m/s$ to evaluate the time delay between front and rear wheel this will give a delay of $.25\Omega^{'} rad$.

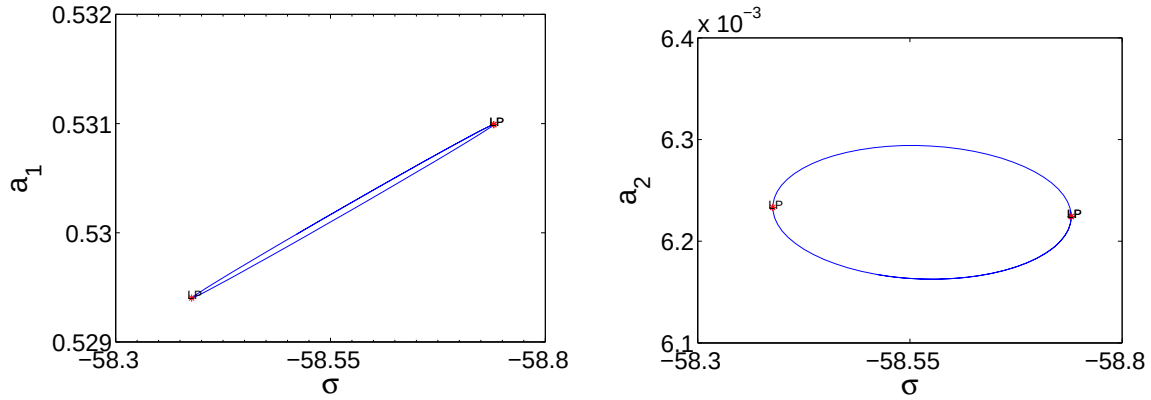

(a) (b)

Figure 4.3: Frequency response curves (a) a_1 vs σ and (b) a_2 vs σ

We have plotted the envelope equations using the MATCONT tool. The equilibrium curve from converged solution of the envelope equations is plotted for amplitude versus frequency of excitation. We have an isolated limit cycles formed as amplitude vs frequency response curves. The limit points are the points where the vertical line will be tangent to the equilibrium curve. The limit points in Fig. 4.3(a) for a_1 vs σ are observed at the coordinates (-58.74,0.531) and (-58.39,0.5294). And in Fig. 4.3(b) for a_2 vs σ the limit points are observed at (-58.39,0.00623) and (-58.74,0.006226).

4.5 Frequency response results for 1:3 internal resonance

When we consider the 1:3 internal resonance it is clear from the below Figs. that there exists a coupling effect of front wheel amplitude on the rear wheel amplitude.

4.5.1 Primary resonance

The primary resonance is observed when the excitation frequency is same as the natural frequency of the front wheel. While the rear wheel is assumed to have 3 times the natural frequency of the front wheel. In the case of primary resonance the maximum amplitude vs frequency observed on the equilibrium curve (a_1 vs σ_1) at the front wheel in the Fig. 4.4(a) is (-15.15,0.2701). When we consider the coupling effect of front wheel on rear wheel the maximum amplitude vs frequency observed on the equilibrium curve (a_2 vs σ_1) at the rear wheel in the Fig. 4.4 is (-0.2388,0.0002289). The maximum amplitude vs frequency observed on the equilibrium curve (a_2 vs σ_2) at the rear wheel in the Fig. 4.4 is (-0.3979,0.00022).

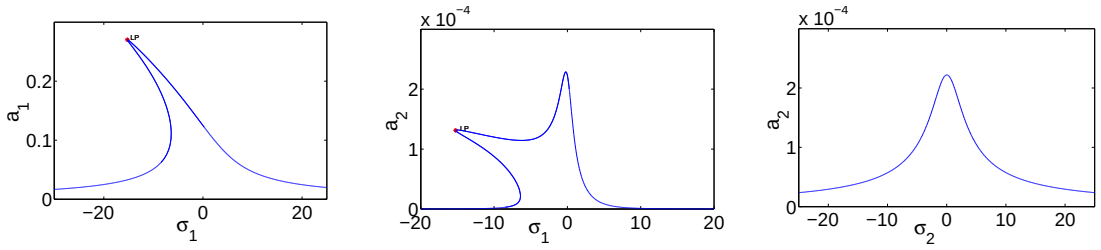

(a) (b) (c)

Figure 4.4: Frequency response curves $\Omega^{'} = \omega_1 + \epsilon\sigma_1$, $3\omega_1 = \omega_2 - \epsilon\sigma_2$ and $F = 1N$. (a) a_1 vs σ_1 (b) a_2 vs σ_1 (c) a_2 vs σ_2

4.5.2 Superharmonic resonance

The superharmonic resonance is observed when the natural frequency at the front wheel is 3 times the excitation frequency. We also consider 1:3 internal resonance between the front and rear wheels i.e. rear wheel has natural frequency which is 3 times the natural frequency of the front wheel. In the case of superharmonic resonance the maximum amplitude vs frequency observed on the equilibrium curve (a_1 vs σ_1) at the front wheel in the Fig. 4.5(a) is (-21.42,0.1936). When we consider the coupling effect of front wheel on rear wheel the maximum amplitude vs frequency observed on the equilibrium curve (a_2 vs σ_1) at the rear wheel in the Fig. 4.5(b) is (-21.24,0.00003481). The maximum amplitude vs frequency observed on the equilibrium curve at rear wheel (a_2 vs σ_2) in the Fig. 4.5(c) is (0.2579,0.000002807).

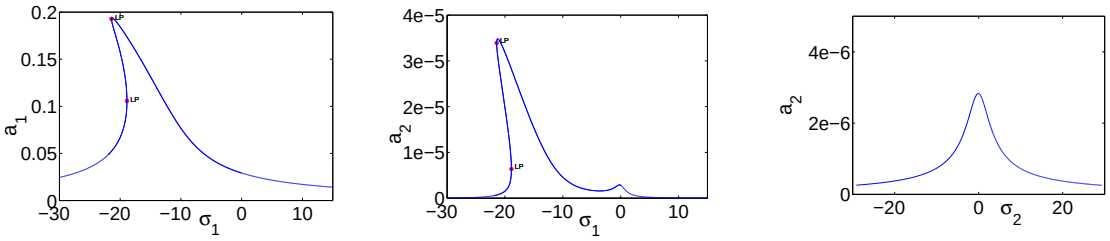

(a) (b) (c)

Figure 4.5: Frequency response curves $3\Omega^{'} = \omega_1 + \epsilon\sigma_1$, $3\omega_1 = \omega_2 + \epsilon\sigma_2$ and $F = 0.16N$. (a) a_1 vs σ_1 (b) a_2 vs σ_1

4.6 Summary

The system is in a 1-1 internal resonance means it has equal natural frequencies at the front and rear portions of the masses i.e. it possesses nonlinear normal modes. We have observed isolated limit cycles for the amplitude frequency curves. In the case of 1:3 internal resonance we have observed clear resonance amplitude on the curves at the frequency of excitation. The peak values on the equilibrium curves are obtained at a particular force at which the system is in equilibrium. The frequency analysis gives an idea about the external force beyond which the system goes to unsteady state and hence to chaotic state.

Chapter 5

Conclusions and Future work

In this thesis, we present the comfort analysis of semi-active and passive dampers using quarter and half car models. To do the analysis, we first described the system response in terms of sprung mass acceleration, suspension stroke, road holding and control force versus vehicle velocity using quarter and half car models with semi-active MR damper. The nonlinear characteristics of MR damper subjected to different current are modeled using the modified Bouc-Wen model. However, we use linearized form of the model to do comfort analysis. On comparing the system response in terms of above parameters at different current, we found that with increasing current, the control force is increased, and the suspension stroke and road holding at front and rear are reduced which in turn give better handling. Adversely, we also found that the sprung mass acceleration increases with increasing current there by reducing the comfort for the passengers in the vehicle. Therefore, it is concluded that there should be limit on he control force as it may increase sprung mass acceleration out-of-bound. To do the nonlinear analysis, we take oil passive with cubic nonlinearity in the half car model. Subsequently, we present two different cases, namely, first, a system with same dampers at front and rare wheels, second, a system with different dampers at front wheel, ω_1, and rear wheel, ω_2, which are having a frequency ratio of three, i.e., $\omega_2 = 3\omega_1$. Finally, we found the nonlinear response for the system subjected to excitation at primary resonance and superharmonic resonance, respectively. It is found that when the same dampers are used, the system gives stable limit cycle over a fixed range of frequencies. For the case of different dampers at front and rare wheels, we get nonlinear coupled response at the rear wheel if front and rare wheels are excited externally with a time delay at ω_1 under primary excitation. Under superharmonic excitation, we excite the system at $\omega_1/3$. In this also we get coupled response at the rear wheel. Moreover, the extent of nonlinearity

increases by increasing the amplitude of excitation. Therefore, the response under large excitation at primary and secondary resonances should be controlled to avoid discomfort to the passenger. MR damper based half car model can be analyzed to control such effects at large excitation amplitude, which forms the basis of the future work.

References

[1] R.S.Prabakar, C.Sujatha, and S.Narayanan. Response of a quarter car model with optimal magnetorheological damper parameters. *Journal of Sound and Vibration* 332, (2013) 2191–2206.

[2] R.S.Prabakar, C.Sujatha, and S.Narayanan. Response of a half-car model with optimal magnetorheological damper parameters. *Journal of Vibration and Control* .

[3] M. S. Siewe. Resonance, stability and period-doubling bifurcation of a quarter-car model excited by the road surface profile. *Physics Letters A* 374, (2010) 1469–1476.

[4] A.Hac. Suspension optimization of a 2-dof vehicle model using a stochastic optimal control technique. *Journal of Sound and Vibration* 100, (1985) 343–357.

[5] B. D. A.G. Thompson. Computation of the rms state variables and control forces in a half-car model with preview active suspension using spectral decomposition methods. *Journal of Sound and Vibration* 285, (2005) 571–583.

[6] Q. Zhu and M. Ishitobi. Chaos and bifurcations in a nonlinear vehicle model. *Journal of Sound and Vibration* 275, (2004) 1136–1146.

[7] Q. Zhu and M. Ishitobi. Chaotic vibration of a nonlinear full-vehicle model. *International Journal of Solids and Structures* 43, (2006) 747–759.

[8] L. G. Rao and S. Narayanan. Preview control of random response of a half-car vehicle model traversing rough road. *Journal of Sound and Vibration* 310, (2008) 352–365.

[9] O. Bayrakdar. Random vibration of a road vehicle. Master's thesis, Izmir institute of technology 2010.

[10] B.F.Spencer, S.J.Dyke, M.K.Sain, and J.D.Carlson. Phenomenological model for magnetorheological dampers. *ASCE Journal of Engineering Mechanics* 123, (1997) 230–238.

[11] Y.K.Wen. Equivalent Linearization for Hysteretic Systems Under Random Excitation. *Journal of Applied Mechanics* 47, (1980) 150–154.

[12] S. Dobson, M. Noori, Z. Hou, M. Dimentberg, and T. Baber. Modeling and random vibration analysis of SDOF systems with asymmetric hysteresis. *International Journal of Non-Linear Mechanics* 32, (1997) 669–680.

[13] F. Tyan, Y.-F. Hong, S. Tu, and W. S. Jent. Generation of random road profiles. *Journal of Advanced Engineering* 1373–1378.

[14] M. Ahmadian and E. Blanchard. Non-dimensionalised closed form parametric analysis of semi-active vehicle suspensions using a quarter-car model. *Vehicle System Dynamics: International Journal of Vehicle Mechanics and Mobility* 49, (2011) 219–235.

[15] M. Ahmadian and C. A. Pare. A Quarter-Car Experimental Analysis of Alternative Semiactive Control Methods. *Journal of Intelligent Material Systems and Structures* 11.

[16] S.Senthil and S.Narayanan. Optimal preview control of a two dof vehicle model using stochastic optimal control theory. *Vehicle System Dynamics* 25, (1996) 413–430.

[17] G. Litak, M. Borowiec, M. I. Friswell, and K. Szabelski. Chaotic vibration of a quarter-car model excited by the road surface profile. *Communications in Nonlinear Science and Numerical Simulation* 13, (2008) 1373–1383.

[18] R. D. Naik and P. M. Singru. Resonance, stability and chaotic vibration of a quarter-car vehicle model with time-delay feedback. *Communications in Nonlinear Science and Numerical Simulation* 16, (2011) 3397–3410.

[19] A. H. Nayfeh and D. T. Mook. Nonlinear Oscillations. 2004th edition. Wiley, Germany, 2004.

[20] J. J. Thomsen. Vibrations and Stability Advanced Theory, Analysis and Tools. Springer, Germany, 2003.

[21] R. Seydel. Practical Bifurcation and Stability Analysis. Springer, USA, 2010.

[22] B. D. Anderson and J. B. Moore. Linear optimal control. Prentice hall inc., Newjersey, USA, 1971.

[23] W. Gao, N. Zhang, and H. P. Du. A half-car model for dynamic analysis of vehicles with random parameters. In 5th Australasian Congress on Applied Mechanics, ACAM. Brisbane, Australia, 2007 .

[24] E. Obialero. A Refined Vehicle Dynamic Model for Driving Simulators. Master's thesis, Chalmers university of technology, Gteborg, Sweden 2013.

[25] G. Taffo and M. S. Siewe. Parametric resonance, stability and heteroclinic bifurcation in a nonlinear oscillator with time-delay: Application to a quarter-car model. *Mechanics Research Communications* 52, (2013) 1–10.

[26] A. F. Vakakis. Fundamental and Subharmonic Resonances in a System with a '1-1' Internal Resonance. *Nonlinear Dynamics* 3, (1992) 123–143.

[27] P. Prakash. Experimental and Analytical Studies of MR Damper under Dynamic Loading. Master's thesis, Indian Institute of Technology Hyderabad, India 2014.

[28] R.S.Prabakar, C.Sujatha, and S.Narayanan. Optimal semi-active preview control response of a half car vehicle model with magnetorheological damper. *Journal of Sound and Vibration* 326, (2009) 400–420.